Preprints of the 21st IFAC World Congress (Virtual)
Berlin, Germany, July 12-17, 2020

Equilibrium Manifolds in 2D Fluid Traffic Models ⋆⋆

Liudmila Tumash * **Carlos Canudas-de-Wit** *
Maria Laura Delle Monache **

* *Univ. Grenoble Alpes, CNRS, Inria, Grenoble INP, GIPSA-lab, 38000 Grenoble, France.*
** *Univ. Grenoble Alpes, Inria, CNRS, Grenoble INP, GIPSA-lab, 38000 Grenoble, France.*

Abstract: The main goal of this paper is to analytically find a steady-state in a large-scale urban traffic network with known and constant demand and supply on its boundaries. Traffic dynamics are given by a continuous two-dimensional macroscopic model, where state corresponds to the vehicle density evolving in a 2D plane. Thereby, the flux magnitude is given by the space-dependent fundamental diagram and the flux direction depends on the underlying network topology. In order to find a steady-state, we use the coordinate transformation such that the 2D equation can be rewritten as a parametrized set of 1D equations. This technique allows us to obtain the curves along which the traffic flow evolves, which are essentially the integral curves of the flux field constructed from the network geometry. The results are validated by comparing the obtained steady-state with the one estimated by using a microsimulator.

Keywords: Urban systems, Partial differential equations, Steady states, Road traffic, Differential geometric methods.

1. INTRODUCTION

The first macroscopic model describing the behaviour of traffic as fluid was the Lighthill, Whitham and Richards model, or simply LWR (Lighthill and Whitham (1955); Richards (1956)). It describes the spatio-temporal evolution of traffic density on a single link (a road) by a scalar conservation law. Its main assumption is the existence of a relation between the vehicles' density and their flow (fundamental diagram). Despite the appearance of more sophisticated models capturing more complex traffic phenomena (Aw and Rascle (2000); Greenberg et al. (2003)), the LWR model remains the most popular one due to its simplicity. To enable comparison of different models or to solve optimal boundary control tasks, it is essential to investigate the steady-state solution, which will be the main goal of this paper. For the case of classical 1D LWR. For a $1D$ inhomogeneous case (one road with bottlenecks) this was done in (Wu et al. (2014)), using the conditions derived in (Zhang and Liu (2003)) that ensure the unique physically relevant solution. However, in case of 2D traffic modelling this problem wasn't considered so far.

In the sixties there were made first attempts to describe traffic state on urban networks (Smeed (1966); Thomson (1967); Herman and Prigogine (1979)). However, their models failed to capure traffic's behaviour in a rush hour. Geroliminis and Daganzo (2008) observed a congested urban network in Yokohama and experimentally established the existence of a macroscopic fundamental diagram (MFD) relating average flow and average density on a large urban area, which was generalized in (Daganzo and Geroliminis (2008)). Due to this finding, reservoir models describing temporal evolution of vehicles' accumulation in some urban zone can be used. However, MFD is well defined only in areas consisting of links with a similar level of congestion, although many real transportation networks are heterogeneous. To overcome the problem, Hajiahmadi et al. (2013); Leclercq et al. (2015) presented algorithms of partitioning an urban area into multiple homogeneous zones each having its own well-defined MFD. However, even these accumulation models with partition capture poorly the spatial distribution of traffic flow, which makes them limited for model-based control design.

Another way to model traffic in large-scale urban networks is to use two-dimensional continuous models. In this paper we will work with the 2D-LWR model presented in (Mollier et al. (2018)). Instead of calculating the number of cars in different zones using MFD, the 2D-LWR model implements the space-dependence into the fundamental diagram, whose parameters can be estimated from the network topology. Thus, this model captures quite well the changing traffic conditions such as in- and outflow.

The main contribution of this paper is a model-based steady-state computation for a two-dimensional conservation law describing traffic on a large-scale urban area. This has never been done before. The steady-state solution will depend only on network topology and demand and supply on its boundary. For this we will introduce some coordinate transformation, as well as use the result from (Wu et al. (2014)) to extract the density from the steady-state flow.

⋆ First author's e-mail: liudmila.tumash@gipsa-lab.fr.
⋆⋆This work was supported by the funding from the European Research Council (ERC) under the European Union's Horizon 2020 research and innovation programme (grant agreement 694209)

2. MODEL

The evolution of traffic in urban areas can be described by a two-dimensional continuous model such as 2D LWR (Mollier et al. (2018)), where the state corresponds to the traffic density $\rho(x, y, t)$. Its dynamics are based on the conservation of the number of cars in a 2D plane:

$$\begin{cases} \dfrac{\partial \rho(x,y,t)}{\partial t} + \nabla \cdot \mathbf{\Phi}(x, y, \rho(x, y, t)) = 0, \quad \forall t \in \mathbb{R}^+ \\ \rho(0, x, y) = \rho_0(x, y), \quad \forall (x, y) \in D \end{cases} \tag{1}$$

where D is a compact domain corresponding to the urban area we consider, and

$$\mathbf{\Phi} = \phi(x, y, \rho)\boldsymbol{d}_\theta(x, y), \tag{2}$$

is a flow vector function, where ϕ is the flow's magnitude determined by a space dependent *fundamental diagram* (FD):

$$\phi(x, y, \rho) = v(x, y, \rho)\rho = v_{max}(x, y)\Psi\left(\frac{\rho}{\rho_{max}(x, y)}\right)\rho, \tag{3}$$

where $\Psi(\rho/\rho_{max})$ is the velocity function depending on density, e.g., for Greenshields FD $\Psi(\rho/\rho_{max}) = 1 - \rho/\rho_{max}$ (Greenshields et al. (1935)). The flow magnitude $\phi(x, y, \rho) : [0, \rho_{max}(x, y)] \to \mathbb{R}^+$ is a Lipschitz continuous and concave function with a space-dependent maximum $\phi_{max}(x, y)$ (*capacity*) achieved at $\rho_c(x, y)$ (*critical density*). In Section 4.2 we will explain how to determine these parameters from network's topology. We also distinguish two density regimes: $\Omega_f := [0, \rho_c]$ indicates the *free-flow regime*, and $\Omega_c := (\rho_c, \rho_{max}]$ stays for the *congested regime*. In the free-flow regime vehicles move freely with positive kinematic wave speed, while in the congested regime vehicles move slowly with negative kinematic wave speed.

Further, in (2) $\boldsymbol{d}_\theta(x, y) = (\cos(\theta(x, y)), \sin(\theta(x, y)))$ is a direction vector determined by network's topology. We will call it the flux field, since it corresponds to the vector field along which the flow (3) evolves. Thus, the flow vector function (2) can be rewritten as:

$$\mathbf{\Phi} = \phi(x, y, \rho)\begin{pmatrix} \cos(\theta(x, y)) \\ \sin(\theta(x, y)) \end{pmatrix}. \tag{4}$$

3. PROBLEM STATEMENT

Define Γ as the boundary of domain D. Then, we define its subset $\Gamma_{in} \subset \Gamma$ as a set of boundary points (x, y) for which $\boldsymbol{n}(x, y) \cdot \boldsymbol{d}_\theta(x, y) > 0$, where $\boldsymbol{n}(x, y)$ is a unit normal vector to the boundary, oriented inside the domain. In a similar way, we also define $\Gamma_{out} \subset \Gamma$ such that $\forall (x, y) \in \Gamma_{out}$: $\boldsymbol{n}(x, y) \cdot \boldsymbol{d}_\theta(x, y) < 0$.

Assume that we know inflow demand $D_{in}(x, y)$ $\forall (x, y) \in \Gamma_{in}$ and outflow supply $S_{out}(x, y)$ $\forall (x, y) \in \Gamma_{out}$, where inflow demand and outflow supply are used to denote the number of cars per hour that want to enter and are able to exit the domain, respectively. We want to develop a technique that yields the steady-state of (1) analytically. This is formalized as follows:

Problem 1. Given some constant $D_{in}(x, y)$ $\forall (x, y) \in \Gamma_{in}$ and constant $S_{out}(x, y)$ $\forall (x, y) \in \Gamma_{out}$, and the traffic state with dynamics given by (1), find a time-invariant density distribution $\rho^*(x, y)$ such that

$$\nabla \cdot \mathbf{\Phi}(x, y, \rho^*(x, y)) = 0. \tag{5}$$

4. PRELIMINARIES

In this part we will motivate the use of 2D-LWR for steady-state estimation. For this purpose we will run a scenario on a Manhattan grid with slightly disordered positions of nodes for 2D-LWR (1) and for a reservoir model that is related to the existence of a Macroscopic Fundamental Diagram (MFD). A key advantage of MFD is that it does not require high computational effort.

4.1 Macroscopic Fundamental Diagram

MFD describes the evolution of accumulation of vehicles in a zone as described in (Aboudolas and Geroliminis (2013)). Consider a heterogeneous network partitioned in N reservoirs. Let $n_i(t)$ be the accumulation of vehicles in reservoir i at time t. The main assumption of the accumulation model is the existence of $\phi_i(n_i(t))$, which relates the number of cars in a reservoir i with outflow $\phi_{i,out}$. Let us also define $\mathcal{N}_{in,i}$ as a set of neighbouring reservoirs, whose cars can directly reach reservoir i, and $\mathcal{N}_{out,i}$ as a set of neighbouring reservoirs which can be directly reached by the cars from reservoir i (see Fig. 1). Then, the number of cars in i can be described as:

$$\begin{aligned} \frac{dn_i(t)}{dt} &= \phi_{in,i}(t) - \phi_{out,i}(t), \quad \text{with} \\ \phi_{in,i}(t) &= \sum_{j \in \mathcal{N}_{in,i}} r_{ji} \min\left(D_j, S_i\right) \quad \text{and} \\ \phi_{out,i}(t) &= \sum_{j \in \mathcal{N}_{out,i}} r_{ij} \min\left(D_i, S_j\right), \end{aligned} \tag{6}$$

where r_{ji} is the number of the roads from a neighbouring reservoir j to reservoir i; D_j and S_i are the demand and the supply function in j and i, respectively, defined as

$$\begin{aligned} D_i(n_i(t)) &= \begin{cases} \phi_i(n_i(t)) & \text{if} \quad n_i < n_{c,i} \\ \phi_{max,i}, & \text{if} \quad n_i \geq n_{c,i} \end{cases} \\ S_i(n_i(t)) &= \begin{cases} \phi_{max,i} & \text{if} \quad n_i \leq n_{c,i} \\ \phi_i(n_i(t)), & \text{if} \quad n_i > n_{c,i} \end{cases} \end{aligned} \tag{7}$$

MFD for each reservoir was computed using the GPS data

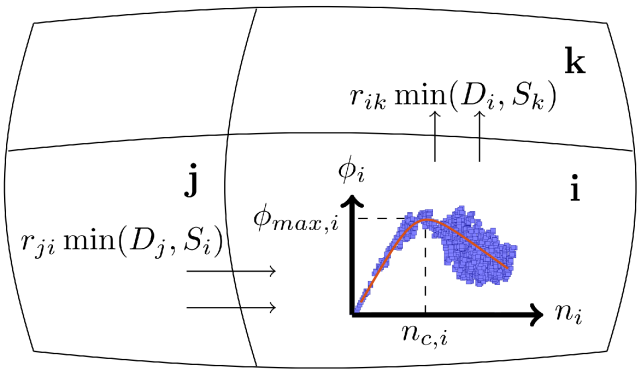

Figure 1. Schematic illustration of a network with $N = 4$ zones. The variables are defined with respect to reservoir i, which has its own MFD (fitted data, in red) $\phi_i(n_i)$ with the maximum flow $\phi_{max,i}$ attained at the critical number of cars $n_{c,i}$. The change in vehicle's accumulation $n_i(t)$ is determined by flows from $\mathcal{N}_{in,i} = \{j\}$ and by flows into $\mathcal{N}_{out,i} = \{k\}$.

(velocities) from microsimulator at each t:

$$\phi_i(n_i(t)) = \left(\frac{1}{n_i}\sum_{m=1}^{n_i(t)} v_{im}\right)\left(\frac{n_i}{\sum\limits_i l_i}\right) = \frac{1}{\sum\limits_i l_i}\sum_{m=1}^{n_i(t)} v_{im},$$

where $\sum\limits_i l_i$ corresponds to the length of all roads in reservoir i, m is the index used to denote the vehicle in reservoir i, and v_{im} is the velocity of vehicle m in reservoir i. Having data in form (n_i, ϕ_i), we fit a cubic polynomial as in (Aboudolas and Geroliminis (2013)) and extract the maximal flow $\phi_{max,i}$. The maximal density ρ_{max} is calculated as one vehicle divided by the minimal distance between two consecutive vehicles ($d_{min} = 6$m).

Aboudolas and Geroliminis (2013) present a method to make a network partition based on the traffic state. However, to make a fair comparison, we will perform a partition into sixteen equal parts, since the goal of this work is to develop a topology-based method of steady-state reconstruction.

The steady-state in reservoir model is reached when $dn_i(t)/dt = 0\ \forall i \in \{1...N\}$. This means that by (6) we obtain for each reservoir i:

$$\phi^*_{in,i}(t) = \phi^*_{out,i}(t), \tag{8}$$

where the asterisk is used to denote the steady-state.

We will compare steady-states obtained by both models (1) and (6) with the one obtained by microsimulator Aimsun, which simulates the dynamics of vehicles' positions in an urban area. To enable comparison, we will reconstruct the density from vehicles' positions using the Kernel Density Method as described in (Mollier et al. (2018)).

Finally, we define the following metric Q of proximity of the model to the "ground truth":

$$Q = \sqrt{\int_0^{x_{max}}\int_0^{y_{max}} (\rho_i(x,y) - \rho_{sim}(x,y))^2\, dxdy}, \tag{9}$$

where x_{max} and y_{max} are the maximal values of the domain, ρ_i is the density corresponding to the model we compare, i.e., the one from 2D-LWR (1), from MFD (piecewise constant function reconstructed from vehicles' accumulation etc.), and ρ_{sim} is the density from microsimulator Aimsun. Thus, Q yields the L^2 difference of densities.

4.2 Network Description

We consider a 10×10 or 1km square Manhattan grid (see Fig. 5, where the nodes are indicated in grey). Positions of nodes (intersections) are slightly disordered with white noise of standard deviation 10m. We assume that all roads are single-lane and are globally oriented towards the North-East direction. The network contains a topological bottleneck in the middle, e.g., a river with some bridges. The speed limits on most of the roads are set to 30 km/h, and there are also two roads with 50 km/h.

Since we work with a continuous model (1), we need to reconstruct the flux field $\boldsymbol{d}_\theta(x,y)$, the maximal velocity $v_{max}(x,y)$, and the maximal density $\rho_{max}(x,y)\ \forall (x,y) \in D$. We do it by the Inverse Distance Weighting as in (Mollier et al. (2018)) additionally assuming that the flux field depends on the speed limit. Introduce β as a parameter measuring the sensitivity of the flux field $\boldsymbol{d}_\theta(x,y)$ to the mutual location of roads in a network. For the density reconstruction we chose $\beta = 20$, which means that we want the flux to follow only the global trend of direction of all roads, see Section 2.2 (Mollier et al. (2019)) for a detailed explanation of parameter β.

4.3 Scenario Description

In order to obtain a steady-state, we run a dynamic scenario on microsimulator Aimsun for the network described above for 2 hours of simulator time. Thereby, we see that the density shape does not change much after a certain time interval indicating that the steady-state was reached.

The domain contains 15 in-coming roads on the boundary (8 on the left and 7 on the bottom boundary, respectively). Thereby, at each time step we provide very big demand in the South-West region of the area ($D_{in} = 1200$ veh/h on all 8 in-coming roads, i.e., 4 on the bottom and 4 on the left boundaries) and a lower demand in the rest of the area ($D_{in} = 300$ veh/h on the rest 7 in-coming roads, i.e., 3 on the bottom and 4 on the left boundaries). Thus, congestion is created in almost the whole Western part of the network.

The turning ratios at each 2×2 intersection is 75% turn and the rest 25% continue moving straightforward, while at each 1×2 intersection the turning ratios are 50%.

During the simulation we save the position of all cars at each time step. Finally, from the vehicles' positions we reconstruct a two dimensional density using the Kernel Density Method (see Section 3.3 of (Mollier et al. (2018)) for a detailed description). In short, the assumption is that each vehicle contributes to the global density with a Gaussian kernel centred in its position. We assume that each vehicle contributes to the density for $d_0 = 50$m, where d_0 is the standard deviation of the Gaussian. The same is done at the boundary for the inflow demand (but in 1D). We set the headway between two consecutive cars to 6m.

Finally, we implement the numerical method described in Section 4.1 in (Mollier et al. (2018)) to model the scenario for (1). MFD was solved numerically using Euler method.

4.4 MFD vs Microsimulator

In Fig. 2 we observe a steady-state reconstructed from Aimsun (right panel) and from MFD (left panel). For MFD we performed a partition in 16 areas and depicted the number of cars obtained by (6) at each area. Before we calculate the metric Q, it is reasonable to obtain the value of density in each reservoir $i \in \{1...N\}$ as:

$$\rho_{mfd}(x,y) = \frac{n^*_i}{s_i}, \quad \text{where} \quad i : (x,y) \in R_i, \tag{10}$$

where s_i is the square (in m^2) of reservoir with index i, and R_i is the domain taken by this reservoir.

Thus, using (10) and (9), we obtain $Q = 0.58$. We see that MFD is able to capture the phenomenon of congestion in zones where it arises. However, this model is discrete in space and, by its nature, in does not allow to develop model-based control approaches. As reservoirs' areas enlarge, the performance of the model degrades.

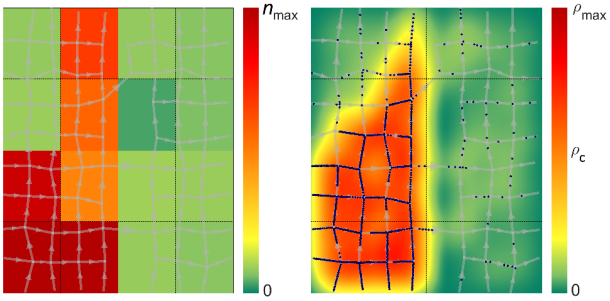

Figure 2. Steady-states obtained by MFD (left) and the one obtained from the microsimulator (right). Gray arrows denote one-way directed roads of the urban zone. Blue filled circles represent vehicles.

4.5 2D-LWR vs Microsimulator

Further, in Fig. 3 we observe a steady-state density reconstructed from Aimsun (right) and 2D-LWR (left). Using our metric (9), we obtain $Q = 0.38$, which is significantly smaller than in the case with MFD. Thus, the steady-state obtained by numerical simulation of (1) captures quite well the spatial distribution of congestion. Thus, it is totally reasonable to use this model for analytical steady-state computation as stated in Problem 1.

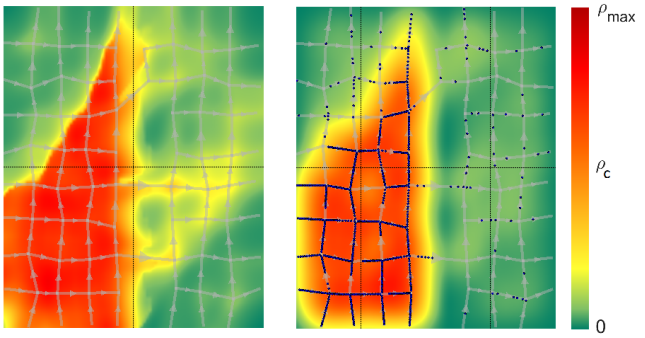

Figure 3. Steady-states obtained by 2D-LWR (left) and the one obtained from the microsimulator (right).

5. ANALYTICAL COMPUTATION OF THE STEADY-STATE OF 2D MODEL

To find a steady-state $\rho^*_{x,y}$, we propose to rewrite (1) from 2D into a parametrized set of 1D equations using coordinate transformation. Then, it will be possible to easily identify the actuation boundaries for the density control at some point or domain. Model (1) can be simplified, since the flux field $\boldsymbol{d}_\theta(x,y)$ does not depend on the state.

5.1 Coordinate Transformation

To obtain a set of 1D equations, we define new coordinates (ξ,η) by rotating and rescaling the differentials dx and dy, i.e.:

$$\begin{pmatrix} d\xi \\ d\eta \end{pmatrix} = C(_\theta(x,y) R_\theta(x,y) \begin{pmatrix} dx \\ dy \end{pmatrix} \tag{11}$$

where $R_\theta(x,y)$ is the rotation matrix

$$R_\theta(x,y) = \begin{pmatrix} \cos\left(\theta(x,y)\right) & \sin\left(\theta(x,y)\right) \\ -\sin\left(\theta(x,y)\right) & \cos\left(\theta(x,y)\right) \end{pmatrix}, \tag{12}$$

where θ is the flow angle as defined in (4), and $C(x,y)$ is the scaling matrix given by

$$C(x,y) = \begin{pmatrix} \alpha(x,y) & 0 \\ 0 & \beta(x,y) \end{pmatrix} \tag{13}$$

where $\alpha(x,y)$ and $\beta(x,y)$ are positive and bounded scaling parameters used to make the metric normalized and uniformly distributed in (ξ,η)-space. In particular, α and β are related to the scaling between the lines of constant ξ and between the lines of constant η, respectively. In (ξ,η)-space the flow evolves only along lines of constant η, as it will be shown in the next subsection. See Fig. 4 for more intuition on how such differentials are related.

For the explicit form of ξ and η, we must take an integral along the path of $(d\xi, d\eta)$ defined in (11). Thereby, we must provide the independence of the chosen integration path, since the integral along any closed curve must be zero. By the theorem of Schwarz this means that the order of taking partial derivatives w.r.t. x and y should be irrelevant, i.e.:

$$\frac{\partial}{\partial y}\left(\frac{\partial \xi(x,y)}{\partial x}\right) = \frac{\partial}{\partial x}\left(\frac{\partial \xi(x,y)}{\partial y}\right), \tag{14}$$

and

$$\frac{\partial}{\partial y}\left(\frac{\partial \eta(x,y)}{\partial x}\right) = \frac{\partial}{\partial x}\left(\frac{\partial \eta(x,y)}{\partial y}\right). \tag{15}$$

Thus, by inserting (11) in (14) and (15), we obtain the equations which must be satisfied for scaling parameters:

$$-\sin\theta\frac{\partial\left(\ln\alpha\right)}{\partial x} + \cos\theta\frac{\partial\left(\ln\alpha\right)}{\partial y} = \cos\theta\frac{\partial\theta}{\partial x} + \sin\theta\frac{\partial\theta}{\partial y} \tag{16}$$

and

$$\cos\theta\frac{\partial\left(\ln\beta\right)}{\partial x} + \sin\theta\frac{\partial\left(\ln\beta\right)}{\partial y} = \sin\theta\frac{\partial\theta}{\partial x} - \cos\theta\frac{\partial\theta}{\partial y} \tag{17}$$

These functions depend only on the direction field $\boldsymbol{d}_\theta(x,y)$ and thus can be precomputed from the network topology.

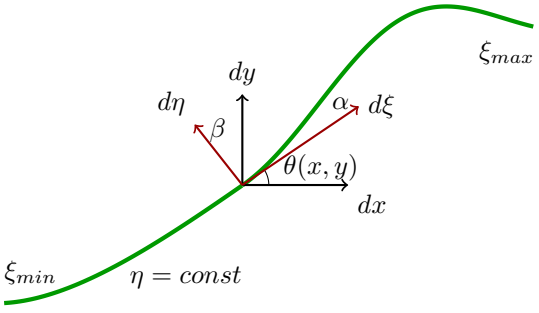

Figure 4. Coordinate transformation for one single η.

5.2 Divergence in (ξ,η)-space

Due to (1), we need to calculate $\nabla\cdot\boldsymbol{\Phi}$ in (ξ,η)-space by applying the divergence formula (Lamé (1859)):

$$\nabla\cdot\boldsymbol{\Phi} = \frac{1}{h_\xi h_\eta}\left[\frac{\partial\left(\boldsymbol{\Phi}_\xi h_\eta\right)}{\partial\xi} + \frac{\partial\left(\boldsymbol{\Phi}_\eta h_\xi\right)}{\partial\eta}\right], \tag{18}$$

where h_ξ and h_η are Lamé coefficients that correspond to the length of the basis vectors in (ξ,η)-space defined as:

$$\boldsymbol{h_\xi} = \left(\tfrac{\partial x}{\partial\xi}, \tfrac{\partial y}{\partial\xi}\right)^T \quad \text{and} \quad \boldsymbol{h_\eta} = \left(\tfrac{\partial x}{\partial\eta}, \tfrac{\partial y}{\partial\eta}\right)^T \tag{19}$$

For the computation of (19), we invert Jacobian (11):

$$\begin{pmatrix} dx \\ dy \end{pmatrix} = \begin{pmatrix} \frac{1}{\alpha}\cos\theta & -\frac{1}{\beta}\sin\theta \\ \frac{1}{\alpha}\sin\theta & \frac{1}{\beta}\cos\theta \end{pmatrix} \begin{pmatrix} d\xi \\ d\eta \end{pmatrix} \tag{20}$$

The combination of (20) and (19) yields:

$$\boldsymbol{h_\xi} = \frac{1}{\alpha}\begin{pmatrix}\cos\theta\\ \sin\theta\end{pmatrix}, \quad \boldsymbol{h_\eta} = \frac{1}{\beta}\begin{pmatrix}-\sin\theta\\ \cos\theta\end{pmatrix} \tag{21}$$

Now we can compute the length of $\boldsymbol{h_\xi}$ and $\boldsymbol{h_\eta}$:

$$h_\xi = |\boldsymbol{h_\xi}| = \frac{1}{\alpha}, \quad h_\eta = |\boldsymbol{h_\eta}| = \frac{1}{\beta} \tag{22}$$

Using (22), we are able to normalize the basis vectors by dividing (21) by their length (22):

$$\begin{cases}\boldsymbol{e}_\xi = \boldsymbol{e}_x\cos\theta + \boldsymbol{e}_y\sin\theta,\\ \boldsymbol{e}_\eta = -\boldsymbol{e}_x\sin\theta + \boldsymbol{e}_y\cos\theta,\end{cases} \tag{23}$$

where $\boldsymbol{e}_x$ and $\boldsymbol{e}_y$ are the basis vectors of (x, y)-space.

Let us now rewrite vector $\boldsymbol{\Phi}$ given by (4) in (ξ, η)-space. Notice that in (x, y)-space this vector reads:

$$\boldsymbol{\Phi} = \phi(x, y, \rho)\cos(\theta(x, y))\boldsymbol{e}_x + \phi(x, y, \rho)\sin(\theta(x, y))\boldsymbol{e}_y. \tag{24}$$

Then by using (23) we obtain:

$$\boldsymbol{\Phi}(x, y, \rho) = \phi(x, y, \rho)\boldsymbol{e}_\xi \tag{25}$$

Thus, the flow evolves along the ξ coordinates, which are tangent to the flow motion, while in the orthogonal direction η there is no motion.

Having Lamé coefficients (22) and the flow vector in (ξ, η)-space (25), we finalize the computation (18) as:

$$\nabla\cdot\boldsymbol{\Phi} = \alpha\beta\left[\frac{\partial(\phi/\beta)}{\partial\xi}\right]. \tag{26}$$

Thereby, η parametrizes the line along which the flow evolves (as a "road"), and set of lines of constant η corresponds to integrated flux field $\boldsymbol{d}_\theta(x, y)$, see Fig. 5.

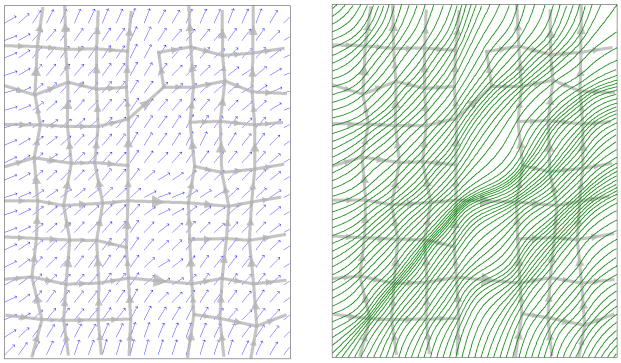

Figure 5. The flux field $\boldsymbol{d}_\theta(x, y)$ from (1) (in blue) and the set of lines of constant η from (28) (in green).

5.3 Simplified model

Using (26), we finally rewrite (1) in (ξ, η) coordinates as

$$\frac{\partial\rho(\xi,\eta)}{\partial t} + \alpha(\xi,\eta)\beta(\xi,\eta)\frac{\partial\left(\phi(\xi,\eta,\rho)/\beta(\xi,\eta)\right)}{\partial\xi} = 0. \tag{27}$$

The obtained system (27) is much more simple than the original model (1). Essentially, it is a 1D model, since the only direction in which the system evolves is ξ.

Using the definition of $\phi(\xi, \eta, \rho)$ in (3), we rewrite (27) as

$$\frac{\partial\left(\frac{\rho}{\alpha\beta}\right)}{\partial t} + \frac{\partial\left(v_{max}\alpha\frac{\rho}{\alpha\beta}\Psi\left(\frac{\rho}{\alpha\beta}/\frac{\rho_{max}}{\alpha\beta}\right)\right)}{\partial\xi} = 0.$$

Defining the rescaled density $\bar\rho = \rho/(\alpha\beta)$, maximal density $\bar\rho_{max} = \rho_{max}/(\alpha\beta)$, flow $\bar\phi = \phi/\beta$ and maximal velocity $\bar v_{max} = v_{max}\alpha$, the latter equation can be rewritten as

$$\frac{\partial\bar\rho(\xi,\eta,t)}{\partial t} + \frac{\partial(\bar v_{max}\Psi(\bar\rho/\bar\rho_{max})\bar\rho)}{\partial\xi} = 0, \tag{28}$$

which is a parametrized 1D-LWR equation with space-dependent FD, i.e., $\bar v_{max}(\xi, \eta)$ and $\bar\rho_{max}(\xi, \eta)$.

5.4 Steady-State Traffic Density

Steady-state solutions to (28) might be nonconstant functions $\bar\rho^*(\xi, \eta)$ due to the space-dependence of fundamental diagram. By the mass conservation law, a steady-state flow in (28) must be constant along the field vector, i.e.:

$$\bar\phi(\eta)^* := \bar v_{max}(\xi,\eta)\Psi(\bar\rho^*/\bar\rho_{max}(\xi,\eta))\bar\rho^*.$$

Assume given demand $D_{in}(\eta)$ and supply $S_{out}(\eta)$. Note that we also need to rescale them by dividing by β:

$$\bar D_{in}(\eta) = D_{in}(\eta)/\beta(\xi_{min}(\eta),\eta),$$
$$\bar S_{out}(\eta) = S_{out}(\eta)/\beta(\xi_{max}(\eta),\eta).$$

Define also $\bar\phi_{max}(\xi,\eta) = \phi_{max}/\beta(\xi,\eta)$ as the maximal possible flow at point (ξ, η) (capacity) with dependence on network topology. In accordance with the analysis in (Wu et al. (2014)), we can write the flow through the "road" as

$$\bar\phi(\eta)^* = \min(\bar D_{in}(\eta), \min_\xi \bar\phi_{max}(\xi,\eta), \bar S_{out}(\eta)), \tag{29}$$

which is the minimum between the demand, the supply and the minimum bandwidth of the system. Note that the steady-state flow of (28) $\bar\phi(\eta)^*$ depends on $\beta(\xi, \eta)$, which indicates the level of compression of the roads.

For each point in the domain and each flow value (except maximal flow), there exist two possible densities: either in the free-flow or in the congested regime. Let us distinguish three possible cases due to (29):

(1) $\bar\phi(\eta)^* = \min_\xi \bar\phi_{max}(\xi,\eta)$. Denote as ξ^* the point where the minimum is achieved. If there are several such points, take the leftmost one (the first one passed by cars). Then the entire domain to the left of ξ^* will be in the congested regime, while the domain to the right will be in the free-flow regime. This is the only solution satisfying the "wave entropy" condition as presented in (Wu et al. (2014); Zhang and Liu (2003)). Thus, the strongest bottleneck creates congestion.
(2) $\bar\phi(\eta)^* = \bar D_{in}(\eta)$: the cars can pass through the system freely (the whole domain is in the free-flow regime).
(3) $\bar\phi(\eta)^* = \bar S_{out}(\eta)$: all the cars are blocked at the exit (the whole domain is in the congested regime).

Finally, we need to retrieve the density by inverting the fundamental diagram in the correct regime and rescale the density back to the original coordinate system:

$$\bar\rho(\xi,\eta) = [\bar\phi^{-1}(\xi,\eta,\cdot)](\bar\phi(\eta)^*),$$
$$\rho(\xi,\eta) = \bar\rho(\xi,\eta)\alpha(\xi,\eta)\beta(\xi,\eta).$$

6. NUMERICAL EXAMPLE

Following all the steps described above, we analytically obtain the steady-state solution of (1), see Fig. 6b). This steady-state solution captures quite well the spatial

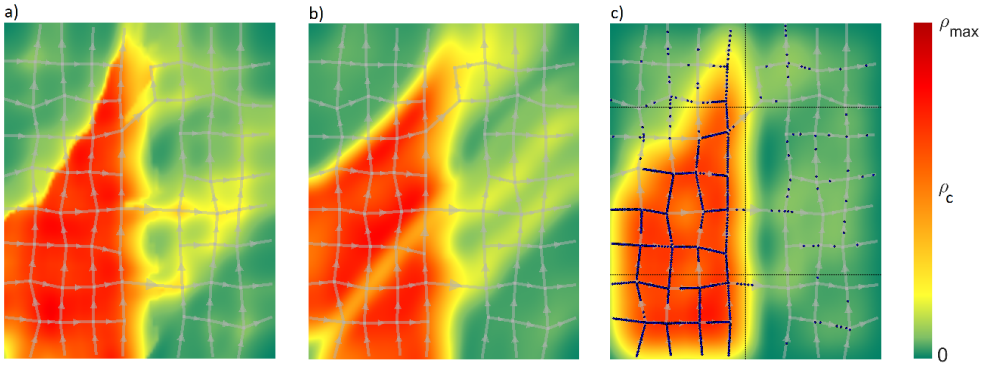

Figure 6. The steady-state density obtained by: a) numerical simulation of 2D-LWR, b) our technique, c) and the one obtained by density reconstruction from the microsimulator.

distribution of congested and free-flow areas, what we can see by comparing our solution with the density obtained by reconstruction from the microsimulator data (Fig. 6c)). In particular, in b) and c) the lines separating congested and free-flow areas in the upper left part are very similar, while in case of steady-state density obtained by numerical simulation (Fig. 6a)) this line lies notably lower. Also by (9) we obtain $Q = 0.40$ for b) , which is almost the same as for a). Thus, we see that our methods yields quire accurate results, which are obtained analytically without any need to run long simulations as in case a).

7. CONCLUSION

In this paper we posed the problem of a model-based steady-state estimation in a continuous 2D traffic system for given inflow demand and outflow supply in a large-scale urban area. We solved this problem analytically by developing a technique that takes inflow demand, outflow supply and maximal flows at each space point and yields the steady-state density. Thereby, we developed a method of coordinate transformation that significantly simplifies the 2D model, making it look as a 1D model, which is simple to work with. The obtained result is in a good agreement with the data from the microsimulator, and it captures better the shape of congested zone in comparison to the result obtained numerically.

ACKNOWLEDGEMENTS

The Scale-FreeBack project has received funding from the European Research Council (ERC) under the European Union's Horizon 2020 research and innovation programme (grant agreement N 694209).

REFERENCES

G. Lamé. Leçons sur les coordonnées curvilignes et leurs diverses applications. Paris, 1859.

B.D. Greenshields, W.S. Channing and H.H. Miller. A study of traffic capacity. *Highway Research Board Proceedings*, vol. 1935, 1935.

M.J. Lighthill and G.B. Whitham. On kinematic waves, II: A theory of traffic flow on long crowded roads. *Proc. Royal Soc. London*, vol. 2, pp. 317–345, 1955.

P.I. Richards Shock waves on the highway. *Operations Research*, vol. 4, pp. 42–51, 1956.

R.J. Smeed The road capacity of city centers. *Traffic Engineering and Control* (7), vol. 8, pp. 455–458, 1966.

J.M. Thomson Speeds and flows of traffic in Central London: 2. Speed-flow relations. *Traffic Engineering and Control* (12), vol. 8, pp. 721–725, 1967.

R. Herman and I. Prigogine A two-fluid approach to town traffic. *Science*, vol. 204, pp. 148–151, 1979.

A. Aw and M. Rascle Resurrection of "second order models" of traffic flow? *SIAM J. Appl. Math.* (30), vol. 60, pp. 916–938, 2000.

J. M. Greenberg, A. Klar and M. Rascle Congestion on multilane highways. *SIAM J. Appl. Math.* (3), vol. 63, pp. 818–833, 2003.

P. Zhang and R.-X. Liu Hyperbolic conservation laws with space-dependent flux: I. Characteristics theory and Riemann problem. *Journal of Computational and Applied Mathematics*, vol. 156, pp. 1–21, 2003.

N. Geroliminis and C.F. Daganzo Existence of urban-scale macroscopic fundamental diagrams: Some experimental findings. *Transportation Research Part B: Methodological* (9), vol. 42, pp. 756–770, 2008.

C. F. Daganzo and N. Geroliminis An analytical approximation for the macroscopic fundamental diagram of urban traffic. *Transportation Research Part B: Methodological* (9), vol. 42, pp. 771–781, 2008.

K. Aboudolas and N. Geroliminis Perimeter and boundary flow control in multi-reservoir heterogeneous networks. *Transp. Res. B: Method.*, vol. 55, pp. 265–281, 2013.

M. Hajiahmadi, V.L. Knoop, B. De Schutter and H. Hellendoorn Optimal dynamic route guidance: A model predictive approach using the macroscopic fundamental diagram. *16th ITSC*, pp. 1022–1028, 2013.

C.-X. Wu, P. Zhang, S.C. Wong and K. Choi Steady-state traffic flow on a ring road with up- and down-slopes. *Physica A*, vol. 403, pp. 85–93, 2014.

L. Leclercq, C. Parzani, V.L. Knoop, J. Amourette and S.P. Hoogendoorn Macroscopic traffic dynamics with heterogeneous route patterns. *Transportation Research Procedia*, vol. 7, pp. 631–650, 2015.

S. Mollier, M.L. Delle Monache and C. Canudas-de-Wit 2D-LWR in large-scale network with space dependent fundamental diagram. *21st Intern. Conf. on Intelligent Trans. Sys. (ITSC)*, Maui, HI, USA, 2018.

S. Mollier, M.L. Delle Monache and C. Canudas-de-Wit Two-dimensional macroscopic model for large scale traffic networks. *Transportation Research B: Methodological*, vol. 122, pp. 309–326, 2019.